High-Resolution C-Arm CT and Metal Artifact Reduction Software: A Novel Imaging Modality for Analyzing Aneurysms Treated with Stent-Assisted Coil Embolization

I. Yuki, Y. Kambayashi, A. Ikemura, Y. Abe, I. Kan, A. Mohamed, C. Dahmani, T. Suzuki, T. Ishibashi, H. Takao, M. Urashima, and Y. Murayama

ABSTRACT

BACKGROUND AND PURPOSE: Combination of high-resolution C-arm CT and novel metal artifact reduction software may contribute to the assessment of aneurysms treated with stent-assisted coil embolization. This study aimed to evaluate the efficacy of a novel Metal Artifact Reduction prototype software combined with the currently available high spatial-resolution C-arm CT prototype implementation by using an experimental aneurysm model treated with stent-assisted coil embolization.

MATERIALS AND METHODS: Eight experimental aneurysms were created in 6 swine. Coil embolization of each aneurysm was performed by using a stent-assisted technique. High-resolution C-arm CT with intra-arterial contrast injection was performed immediately after the treatment. The obtained images were processed with Metal Artifact Reduction. Five neurointerventional specialists reviewed the image quality before and after Metal Artifact Reduction. Observational and quantitative analyses (via image analysis software) were performed.

RESULTS: Every aneurysm was successfully created and treated with stent-assisted coil embolization. Before Metal Artifact Reduction, coil loops protruding through the stent lumen were not visualized due to the prominent metal artifacts produced by the coils. These became visible after Metal Artifact Reduction processing. Contrast filling in the residual aneurysm was also visualized after Metal Artifact Reduction in every aneurysm. Both the observational ($P < .0001$) and quantitative ($P < .001$) analyses showed significant reduction of the metal artifacts after application of the Metal Artifact Reduction prototype software.

CONCLUSIONS: The combination of high-resolution C-arm CT and Metal Artifact Reduction enables differentiation of the coil mass, stent, and contrast material on the same image by significantly reducing the metal artifacts produced by the platinum coils. This novel image technique may improve the assessment of aneurysms treated with stent-assisted coil embolization.

ABBREVIATIONS: MAR = Metal Artifact Reduction; HR = high-resolution

S tent-assisted coil embolization has recently become a common treatment strategy for wide-neck aneurysms.[1-4] However, poor visibility of the deployed stent during the procedure is considered a limitation because digital subtraction angiography does not allow the visualization of many intracranial stents. Ovalization or kinking of the deployed stent in the parent artery is another limitation.[5-8] This phenomenon, also called "inappropri-

ate stent apposition," can hinder the growth of neointimal coverage on the stent.[9] Consequently, treated patients are required to undergo a prolonged postprocedural antiplatelet therapy.

Recent reports show that C-arm CT with contrast has superior spatial resolution compared with conventional CT and allows the visualization of both the deployed stent and the contrast material.[8,10-12] However, once coil embolization is completed, prominent metal artifacts produced by the platinum coils degrade the image quality in the region adjacent to the coil mass, making it extremely difficult to evaluate the minuscule structures around the coil mass.

A new prototype software, Metal Artifact Reduction (MAR; Siemens, Erlangen, Germany), dramatically reduces the metal artifacts in C-arm CT imaging by using a novel image-reconstruction algorithm.[13,14] Combined with currently available high spatial-resolution C-arm CT prototype implementation, the software enables visualization of meticulous structures around highly attenuated materials like platinum coils.

To evaluate the efficacy of MAR, we treated experimental aneurysms with coil embolization by using a stent-assisted technique. Images obtained by using the high-resolution (HR) C-arm CT were processed with MAR. The images before and after MAR processing were compared, and an observational and quantitative analysis was performed.

MATERIALS AND METHODS
Image Acquisition
The images were acquired by using a floor-mounted neuroangiographic unit equipped with 1920 × 2480 cesium iodide–amorphous silicon flat panel detectors covering an area of approximately 30 × 40 cm (Artis zee floor; Siemens). The motorized frontal C-arm, typically used for 3D rotational angiography or soft-tissue-optimized C-arm CT, was used to acquire 496 projection images over a 200° arc (rotation time, 20 seconds) at 80 kV(peak) and a total of 260 mAs. The radiation dose for 1 rotational acquisition ranged from 187 to 233 mGy, depending on the position of the scanned animal and the actual conditions of the scan. The focal spot and source-to-detector distances were 0.3 and 1200 mm, respectively. The objects of interest were positioned at the center of rotation, 750 mm from the source.

To maximize spatial resolution, we used a nonbinned mode instead of the 2 × 2 pixel binning typically used to provide superior contrast resolution for soft-tissue imaging of the C-arm CT. The source projection frames were acquired in a 512 × 512 matrix covering an FOV of 22 cm diagonally. The rotational datasets were processed with a "normal" (or "sharp") kernel type, and each acquisition was reconstructed to 2 volume datasets with a 512 × 512 matrix and an isotropic voxel size ranging from 0.06 to 0.08 mm (corresponding to approximately 30 × 30 mm and 40 × 40 mm FOVs, respectively). The first of these 2 volumes was uncorrected and showed significant metal artifacts, whereas the second featured a metal artifacts correction obtained through the application of the MAR prototype software.

In Vitro Evaluation of the Intracranial Stent by High-Resolution C-Arm CT
To compare the image quality produced by conventional C-arm CT with that of the novel HR C-arm CT, 2 Neuroform stents (4.5 × 20 mm) (Stryker Neurovascular, Kalamazoo, Michigan) were deployed in a silicone vessel model that simulated a bifurcation of a 4-mm vessel. This was scanned by 2 different types of C-arm CT modalities: one with a conventional C-arm CT (Axiom Artis dBA; Siemens), and the other with the high-resolution C-arm CT (Artis zee floor). The 3D volume-rendering images were created by using a Syngo Workplace (Siemens). The obtained 2 images were compared.

Creation of Swine Sidewall Aneurysms followed by Stent-Assisted Coil Embolization
All of the animal experiments were approved by The Jikei University Animal Research Committee. In every treated swine, a sidewall aneurysm was surgically created on each common carotid artery by using a venous graft. Eight experimental aneurysms were created in 6 swine. The aneurysms were designed to be uniformly approximately 6–8 mm in size. To reproduce a wide-neck aneurysm, we adjusted the size of the neck to 4–5 mm in length. The detailed surgical technique was described elsewhere.[15]

After the creation of an aneurysm on each side of the common carotid artery, a 6F short sheath was placed on the right femoral artery. Using the sheath, we advanced a 6F guiding catheter to the ipsilateral common carotid artery and DSA was performed to confirm sufficient contrast filling in the aneurysm. Via the guiding catheter, a microcatheter, Excelsior 1018 (Stryker), was placed in the aneurysm. An intracranial stent was then deployed across the neck of the aneurysm via another microcatheter, Excelsior XT-27 (Stryker).

Three aneurysms were treated with Neuroform EZ stents (Stryker Neurovascular). One aneurysm was treated with an Enterprise stent (Codman & Shurtleff, Raynham, Massachusetts), and 4 were treated with a prototype stent with a closed-cell design (4 × 20 mm). Using a jailing technique, we deployed 3 coils of different sizes into the aneurysms, including Matrix^2 (Stryker), 10 × 30 cm; GDC-10 (Stryker), 6 × 10 cm; and GDC-10, 3 × 6 cm. Every aneurysm was intentionally left underpacked so that the residual aneurysm could be evaluated postoperatively. In 2 aneurysms, part of the deployed coil was intentionally herniated through the stent lumen, to simulate a situation sometimes encountered in the clinical setting.

HR C-Arm CT with Contrast (Intra-Arterial Injection Protocol) followed by MAR Processing
Using the guiding catheter placed at the proximal common carotid artery, we injected 20% diluted contrast material with an injection speed of 2 mL/s for 22 seconds. The image-acquisition-delay time was set at 2 seconds. The raw data of the HR C-arm CT was sent to a postprocessing workstation syngo XWP (Siemens), and the 3D reconstruction of the obtained images was performed by using syngo InSpace software (Siemens). These were saved as the original preprocessing images.

The raw data of the obtained images were then reconstructed by using the MAR prototype software. The post-MAR images were further processed by using an image-processing application, Aquarius iNtuition, Version 4.4.7.108.0 (TeraRecon, San Mateo, California) to build modified volume-rendering images.

Observer Analysis of the Efficacy of MAR Image Processing
Observational analysis of the efficacy of MAR was performed by using a previously reported analytic method.[14] Five independent neurointerventionalists assessed the quality of pre- and post-MAR processed images in a blinded fashion. During the review, observers were allowed to adjust the window-level settings to optimize viewing. The quality of reconstructed images was rated by using a 3-point scale (1 for "insufficient for evaluation," 2 for "sufficient for evaluation," and 3 for "excellent"). Questions included the following: 1) visibility of the stent directly adjacent to the coil mass, and 2) visibility of the parent artery adjacent to the coil mass. Interobserver analyses were performed by using the Wilcoxon signed rank test. Statistical significance was set at a 2-tailed $P = .05$.
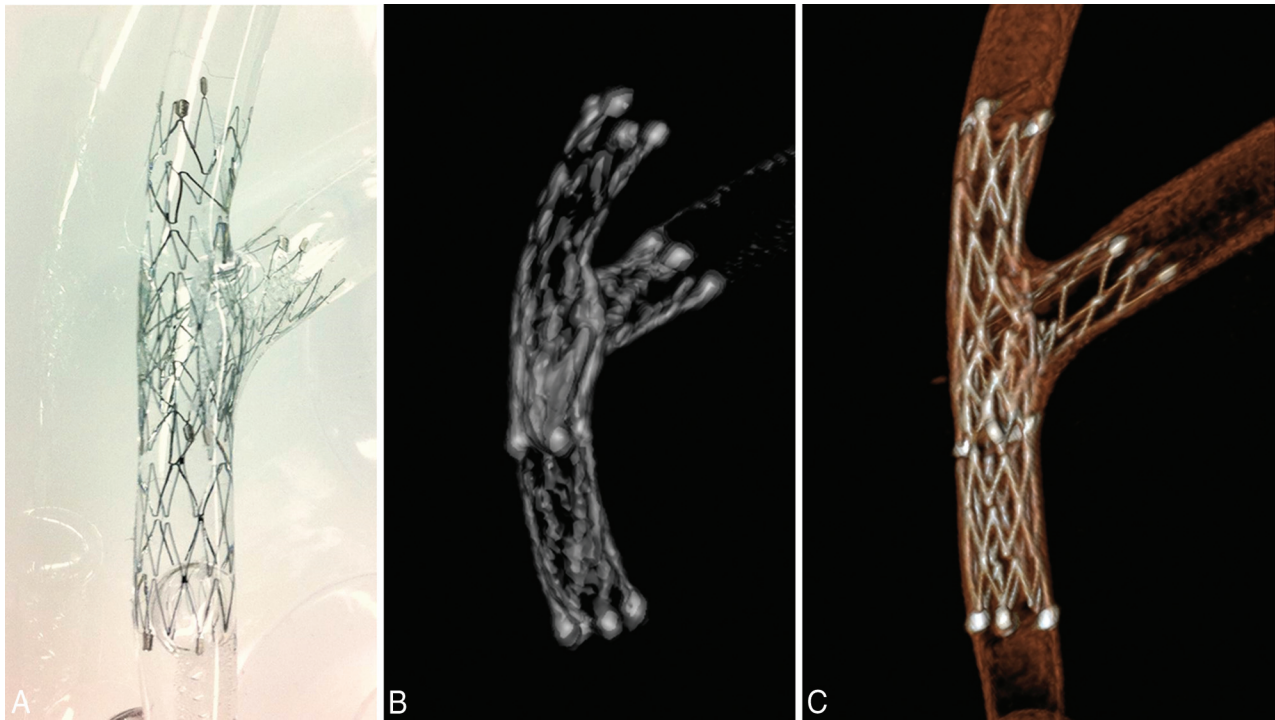
FIG 1. Comparison of the image quality of conventional C-arm CT versus high-resolution C-arm CT. *A*, Two Neuroform stents (4 × 20 mm) are placed at the bifurcation of a silicone vessel model by using a stent-in-stent technique. *B*, The 3D reconstruction image of the conventional C-arm CT. *C*, The 3D reconstruction image of the high-resolution C-arm CT image. Note the improved visualization of meticulous structures of the stent.

Quantitative Analysis of the Efficacy of MAR and HR C-Arm CT

Quantitative analysis of the efficacy of MAR was also performed by measuring the volume of the streak artifacts produced by the coil material. First, by using 3D reconstruction data of a post-MAR image, we created the baseline coil image by setting the window level that provided the best visualization of the coil mass alone. The volume of the metal obtained from this baseline coil image was defined as "baseline metal volume." This volume was calculated by using a free open-source software package for image analysis and scientific visualization (3D Slicer, Version 4.3; http://www.slicer.org).

Second, the window level of the post-MAR image was adjusted for optimal visualization of the parent artery, stent, and coil mass. The same window level was also applied to the pre-MAR image. This adjusted viewing was defined as "optimized visualization" pre- and post-MAR. The volume of the object observed in each of these optimized visualizations (ie, pre- and post-MAR) was then calculated by using the same software, 3D Slicer.

Last, the baseline metal volume was subtracted from each of the pre- and post-MAR volumes, and the differences between the obtained volumes (pre-MAR in optimized visualization minus baseline metal volume and post-MAR in optimized visualization minus baseline metal volume) were considered as the amount of streak artifacts produced by the coil mass.

The average volume of streak artifacts in the pre-MAR images was compared with the average volume calculated in the post-MAR image. Statistical analysis was performed by the Student *t* test. Significance was set at a 2-tailed *P* = .05.

RESULTS

In Vitro Evaluation of the Intracranial Stent by High-Resolution C-Arm CT

A photograph of the Neuroform stents deployed in a silicone vessel model by using the stent-in-stent technique is shown in Fig 1*A*. The image obtained by using the conventional C-arm CT (Fig 1*B*) shows the 2 Neuroform stents (4 × 20 mm) placed in the silicone vessel model with limited visualization of detailed structures (eg, stent struts). The image obtained by the HR C-arm CT (Fig 1*C*) demonstrates the meticulous structures of the deployed stents, including the small gaps between the struts, which were the structural features of the open-cell-design stent.

HR C-Arm CT with Contrast Injection followed by MAR

All 8 aneurysms in the 6 swine were successfully created and were treated by coil embolization by using the stent-assisted technique. Embolization was stopped before complete occlusion of the aneurysm so that the residual aneurysm could be evaluated by post-treatment angiography.

In all aneurysms, thin-section MIP images of the HR C-arm CT obtained immediately after the procedure revealed metal artifacts produced by the coil mass. In the pre-MAR image, the image quality near the coil mass was degraded due to the metal artifacts, and differentiating the coils from the stent was difficult. The thin-section MIP images of the post-MAR image showed reduction of the metal artifacts (Fig 2*A*). The microcatheter placed in the aneurysm via the stent struts became visible after MAR (Fig 2*B*).
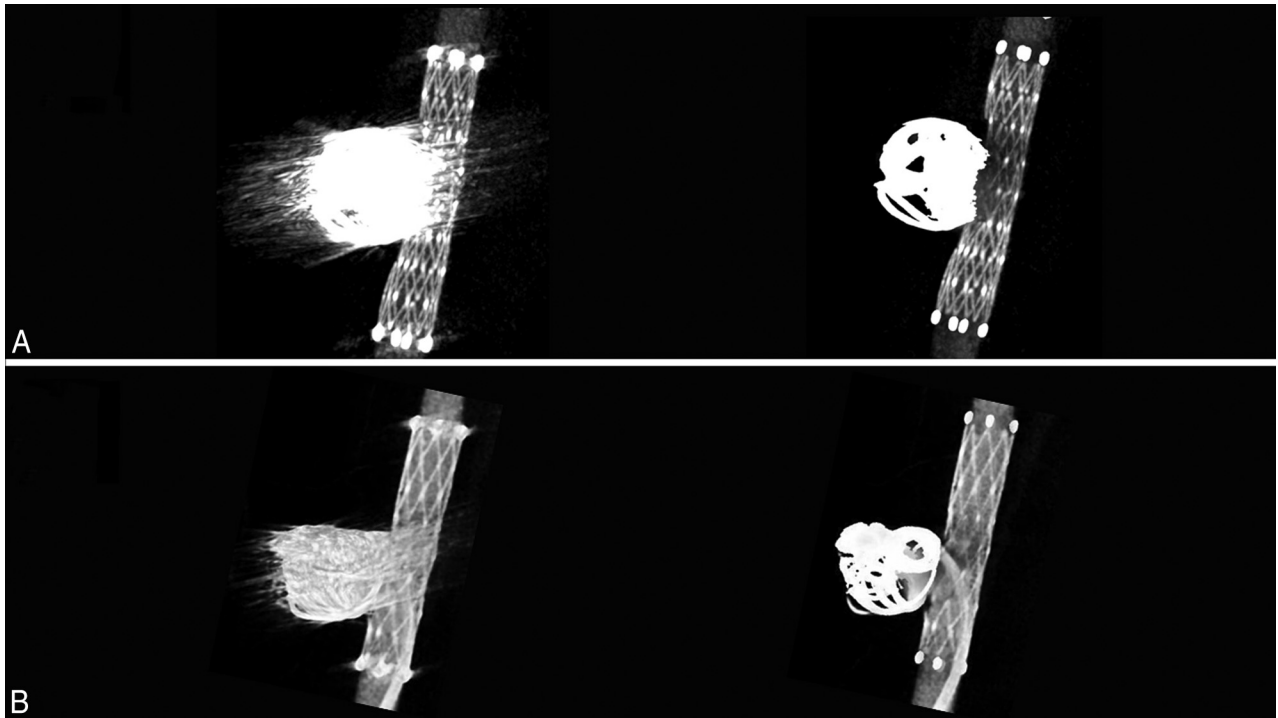
FIG 2. Thin-section MIP images of the aneurysms treated with stent-assisted coil embolization. *A,* Comparison of the pre- (*left*) and post-MAR (*right*) images of an aneurysm treated with a combination of bare platinum coils and a Neuroform stent (4 × 20 mm) reveals improved visibility of the stent structures near the coil mass after MAR processing. *B,* Another aneurysm that was treated with coil embolization by using a Neuroform stent. Note the improved visibility of the microcatheter inserted in the aneurysm and contrast filling in the aneurysm after the MAR processing (*right*).
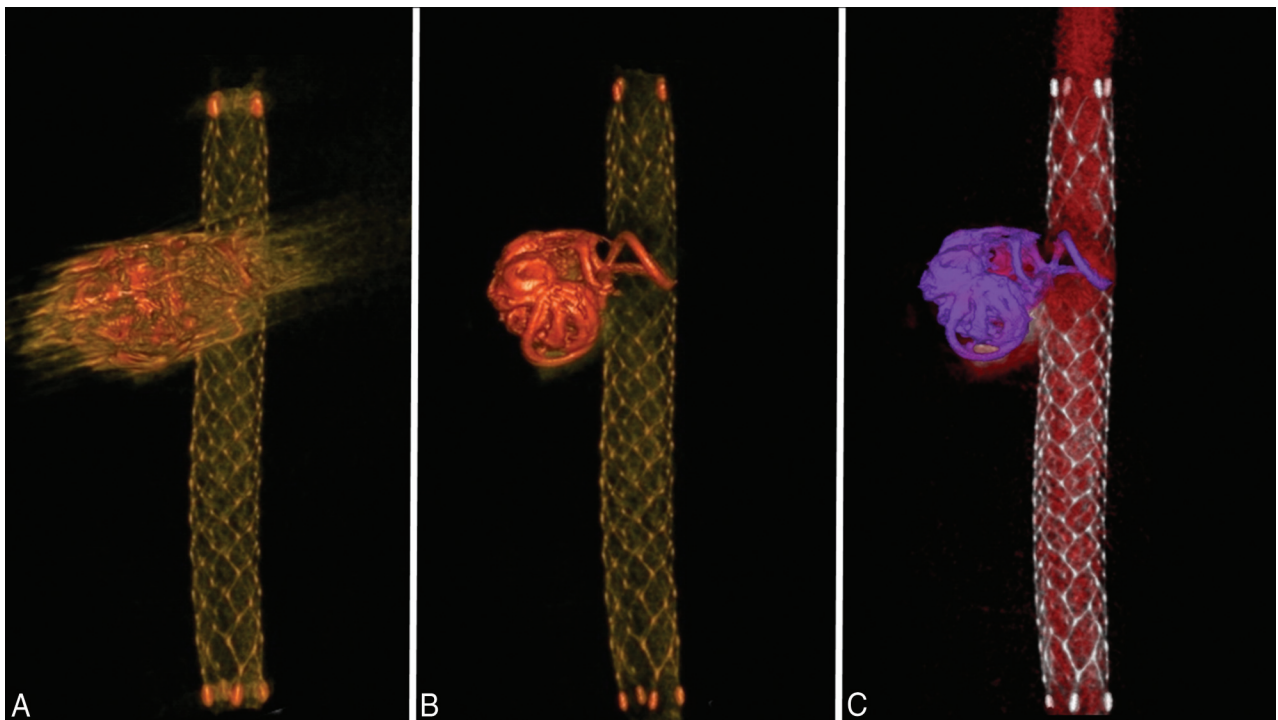

FIG 3. Volume-rendering images of an aneurysm treated by using an Enterprise stent. A volume-rendering image of an aneurysm treated with an Enterprise stent shows that the visibility of the structures around the coil mass in the pre-MAR image (*A*) improves after MAR processing (*B*). *C,* The post-MAR image is further processed by using an image-processing application, Aquarius iNtuition, to create a special volume-rendering image. Different colors are selected on the basis of the range of Hounsfield units. The coil mass (purple) is differentiated from the stent (silver) and contrast (red). The coil loop that protrudes into the stent lumen is also well-visualized.

The volume-rendering images of an aneurysm treated with coil embolization by using an Enterprise stent are shown in Fig 3. Again, the visibility of the structures around the coil mass in the pre-MAR image (Fig 3A) was improved after MAR processing (Fig 3B). The post-MAR image was further processed by using an image-processing application, Aquarius iNtuition, Version 4.4.7.108.0, to build special

volume-rendering images (Fig 3C). The coil mass (purple) is clearly differentiated from the stent (silver), and the coil loop protruding into the stent lumen is clearly visualized.

Observer Analysis of the Efficacy of MAR and HR C-Arm CT

The results of the observer study are summarized in the Table. First, the stent visibility near the orifice of the coil mass was evaluated by using the pooled data analysis. In the pre-MAR images, 77.5% of the samples rated had a score of 1 (insufficient for the diagnosis), while

Results of the observer study rating the visibility of pre- and post-MAR images

Score[a]	Pre-MAR (%)	Post-MAR (%)	Improvement after MAR Wilcoxon Signed Rank Test
Stent visibility			
1	77.5	0.0	Improved after MAR $P < .0001$
2	22.5	40.0	
3	0.0	60.0	
Parent artery visibility			
1	75.0	12.5	Improved after MAR $P < .0001$
2	22.5	30.0	
3	2.5	60.0	
Overall			
1	76.3	6.3	Improved after MAR $P < .0001$
2	22.5	35	
3	1.3	60.0	

[a] Score 1 indicates insufficient for diagnosis; score 2, sufficient for diagnosis; score 3, excellent.

22.5% had a score of 2 (sufficient for the diagnosis). No sample was rated 3 (excellent). In the post-MAR images, 0%, 40%, and 60% of the samples rated had scores of 1, 2, and 3, respectively.

Similarly, the visibility of the parent artery near the coil mass was evaluated. In the pre-MAR images, 75% of the samples rated had a score of 1, 22.5% had 2, and 2.5% had 3. In the post-MAR images, 12.5%, 30%, and 60% of the samples had scores of 1, 2, and 3, respectively.

Overall, in the pre-MAR images, 76.3% of the samples had a score of 1, 22.5% had 2, and 1.3% had 3. In the post-MAR images, 6.3% of the samples had a score of 1, 35% had 2, and 60% had 3.

By the Wilcoxon matched pairs signed rank test, for all categories, the pooled scores given by the observers to the C-arm CT images before MAR were significantly improved after the images were processed with MAR ($P < .0001$).

Quantitative Analysis of the Efficacy of MAR and HR C-Arm CT

The baseline coil image is shown in Fig 4A. Using the workstation syngo Workplace, we adjusted the width and level of the window, the slab thickness, and the position of the images in the post-MAR image (Fig 4B). The same parameters were applied to the pre-MAR image (Fig 4C). The baseline coil volume was subtracted from both the pre- and post-MAR images, and the difference was defined as the "streak artifacts."

The volume of streak artifacts in the pre-MAR images was compared with that in the post-MAR images (Fig 5). In all 8 aneurysms, the volume of streak artifacts calculated in the pre-MAR images was significantly reduced in the post-MAR images. The
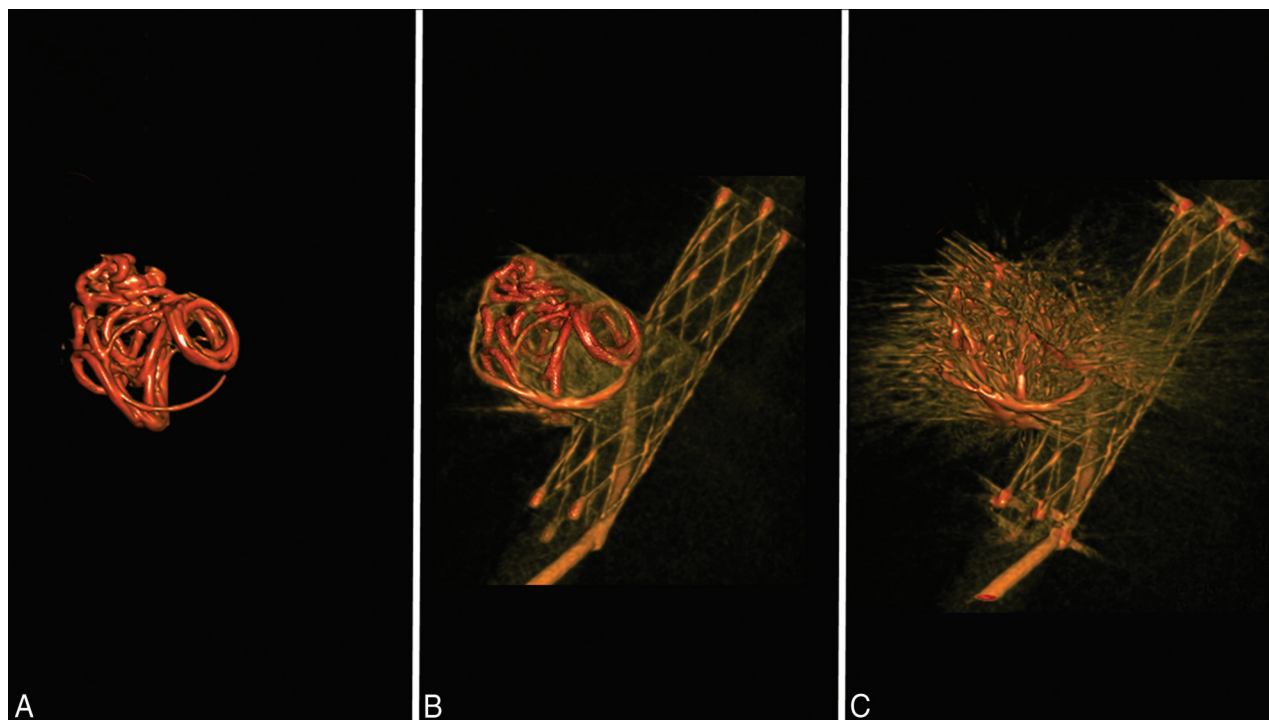

FIG 4. Quantitative measurement of the streak artifacts. *A,* Using the 3D reconstruction data of a post-MAR image, we calculated the baseline metal volume by setting the window level that provides the best visualization of the high-attenuation metal component. *B,* The window level of the post-MAR image is adjusted for the optimal visualization of the parent artery, stent, and coil mass. *C,* The same window level is applied to the pre-MAR image. The volume of the streak artifacts is determined by the difference of the volume of the pre-MAR image and the volume of post-MAR image. The volume of each image is calculated by using the image analysis software 3D Slicer.

Results of Quantitative Analysis:
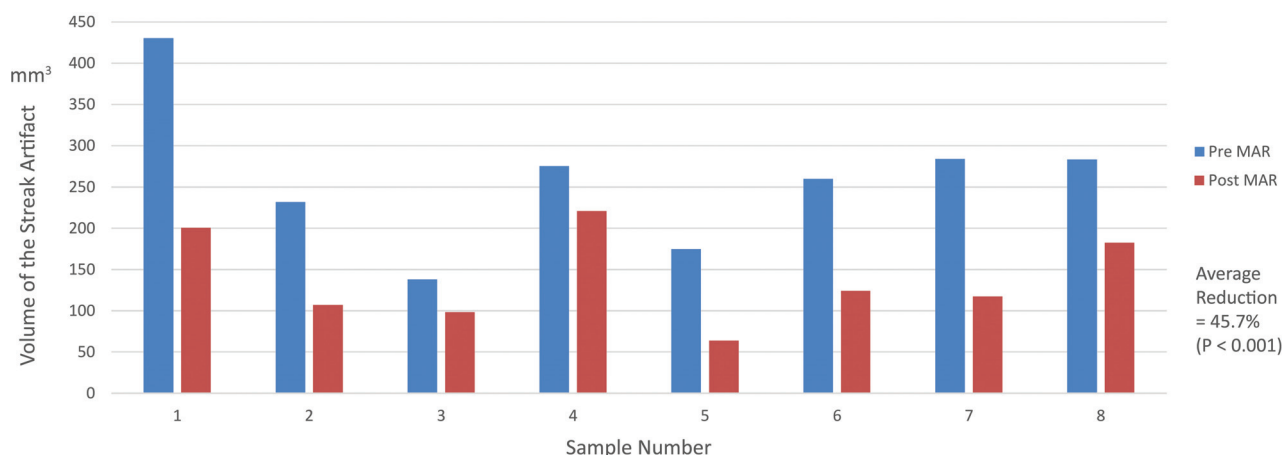## Volume of Streak Artifact

FIG 5. Quantitative analysis of streak artifacts. A graph compares the volume of streak artifacts of the pre- and post-MAR images. In all 8 samples, the volume of streak artifacts in the pre-MAR images is significantly reduced in the post-MAR images. The average artifacts reduction for all samples is 45.7% ($P = .001$).

greatest volume reduction was observed in sample 5, in which the volume of streak artifacts decreased from 174.6 to 63.9 mm^3, yielding a 63.4% artifacts reduction. The lowest volume reduction was seen in sample 4, from 275.1 to 220.8 mm^3, yielding an artifacts reduction of 19.8%. The average artifacts reduction for all samples was 45.7%. By the Student t test, there was a statistically significant difference between the examined datasets ($P = .00034$).

DISCUSSION
Application of Metal Artifact Reduction Software on Currently Available High-Resolution C-Arm CT Images

van der Bom et al[14] reported the efficacy of a metal artifacts correction software on high-resolution C-arm CT images of patients treated with stent-assisted coil embolization. They concluded that the MAR software they used was not capable of fully removing artifacts caused by the implants, even though the image quality of the C-arm CT data was drastically improved after MAR.

The algorithm of the MAR used in the aforementioned study is based on the procedure proposed by Prell et al,[13] whereas the algorithm used in the present work is a modified and extended implementation of the procedure.[16] The main difference is a higher dimension of the matrix used for the reconstruction of the C-arm CT volume (512^3 compared with 256^3), resulting in a potentially higher resolution of the obtained images with relatively smaller voxel sizes for the same FOV. Compared with the currently available normal-resolution C-arm CT images, the quality of the postprocessing images was further improved, allowing better differentiation among the stent, coils, and contrast dye.

Results of the observational analysis revealed significant improvement in the visibility of the meticulous structures after MAR, which was probably due to the prominent reduction in streak artifacts, as shown in the results of the quantitative analysis. Moreover, the high spatial resolution may have contributed to the improved visibility of the minuscule structures after MAR.

Limitations of the Study

The swine aneurysm model used in this study simulates the similar size (of the aneurysm and parent artery) and similar biofluid mechanical parameters (ie, cardiac output and blood viscosity) observed in human aneurysms. However, the parent arteries in human aneurysms are normally more tortuous and are surrounded by a skull. Whether the quality of the images presented in this study can be reproduced in the clinical setting is uncertain.

The effectiveness of the metal artifact reduction can be influenced by the volume and attenuation of the high-attenuating material adjacent to the target vessel. If the stent was surrounded by high-attenuating materials, visualization of the stent will become more challenging. The aneurysm model used in this study was a wide-neck aneurysm, though it does not necessarily represent an extremely wide-neck/fusiform aneurysm. Further study investigating the effectiveness of the MAR in such aneurysms treated with stent-assisted coiling should be conducted.

The quantitative analysis of the metal artifacts focuses on the measurement of the streak artifacts, the high-attenuation radiating artifacts from the coil material that are components of several different types of artifacts, including noise, beam-hardening, partial volume effect, and scatter. Because the streak artifacts are only 1 component of such complex phenomena, establishing a measurement method for the true metal artifacts in reconstructed image data is essential. Notably, the calculated streak artifacts in this study not only include the true artifacts arising from the coil but also the following: 1) part of the stent in the considered volume of interest, 2) the contrast medium in the parent artery confined in that same VOI, and 3) artifacts related to other high-attenuation objects (eg, vertebral bones in the VOI).

One acquisition of the HR DynaCT (Siemens) in this study required a radiation dose of 187–233 mGy. If one knows that 1 biplane DSA acquisition with a frame rate of 4 frames/s and high magnification (eg, 11 cm diagonal) requires approximately 150 mGy, this dose is considered justifiable if the information ob-

tained from the sequence is essential for the decision-making in the course of treatment. However, it is still crucial to minimize the radiation dose by collimating the ROI as much as possible.

Future Applications

When an extremely wide-neck aneurysm or a fusiform aneurysm is treated with a stent-assisted technique, separating the coil mass from the parent artery in the DSA images often becomes difficult. Intraoperative use of the C-arm CT with MAR may allow distinguishing the stent, parent artery, and coils. This distinction may contribute to the prevention of technical complications during the procedure.

Second, to date, most patients undergo prolonged antiplatelet therapy after stent-assisted coil embolization due to the concern of a thromboembolic event related to the deployed stent. In fact, in the field of cardiovascular intervention, studies have shown that inappropriate stent apposition causes delay in neointimal coverage, which can lead to the increased risk of a thromboembolic event.[9]

Intra-arterial sonography or intravascular optical coherence tomography is the imaging modality mainly used for the evaluation of post-coronary stent placement. None of these modalities, however, are currently applicable to the intracranial artery, which is extremely tortuous and vulnerable compared with the coronary artery.

A combination of HR C-arm CT and MAR may contribute to the risk assessment of thromboembolic events related to the stent-assisted coil embolization by providing information about the postoperative stent apposition in the treated artery.

CONCLUSIONS

The combination of currently available high spatial-resolution C-arm CT with a prototype implementation of MAR enables the differentiation of the coil mass, stent, and contrast material by significantly reducing the metal artifacts produced by the platinum coils. This novel image technique allows improved visualization of meticulous structures around the coil mass and may contribute to the evaluation of aneurysms treated with stent-assisted coil embolization.

REFERENCES

1. Chalouhi N, Jabbour P, Singhal S, et al. **Stent-assisted coiling of intracranial aneurysms: predictors of complications, recanalization, and outcome in 508 cases.** *Stroke* 2013;44:1348–53 CrossRef Medline
2. Fiorella D, Albuquerque FC, Deshmukh VR, et al. **Usefulness of the Neuroform stent for the treatment of cerebral aneurysms: results at initial (3–6-mo) follow-up.** *Neurosurgery* 2005;56:1191–201; discussion 1201–02 CrossRef Medline
3. Geyik S, Yavuz K, Yurttutan N, et al. **Stent-assisted coiling in endovascular treatment of 500 consecutive cerebral aneurysms with long-term follow-up.** *AJNR Am J Neuroradiol* 2013;34:2157–62 CrossRef Medline
4. Wakhloo AK, Linfante I, Silva CF, et al. **Closed-cell stent for coil embolization of intracranial aneurysms: clinical and angiographic results.** *AJNR Am J Neuroradiol* 2012;33:1651–56 CrossRef Medline
5. Tsuruta W, Matsumaru Y, Hamada Y, et al. **Analysis of closed-cell intracranial stent characteristics using cone-beam computed tomography with contrast material.** *Neurol Med Chir (Tokyo)* 2013;53: 403–08 CrossRef Medline
6. Heller R, Calnan DR, Lanfranchi M, et al. **Incomplete stent apposition in Enterprise stent-mediated coiling of aneurysms: persistence over time and risk of delayed ischemic events.** *J Neurosurg* 2013;118: 1014–22 CrossRef Medline
7. Heller RS, Malek AM. **Parent vessel size and curvature strongly influence risk of incomplete stent apposition in Enterprise intracranial aneurysm stent coiling.** *AJNR Am J Neuroradiol* 2011;32: 1714–20 CrossRef Medline
8. Patel NV, Gounis MJ, Wakhloo AK, et al. **Contrast-enhanced angiographic cone-beam CT of cerebrovascular stents: experimental optimization and clinical application.** *AJNR Am J Neuroradiol* 2011;32: 137–44 CrossRef Medline
9. Foin N, Gutiérrez-Chico JL, Nakatani S, et al. **Incomplete stent apposition causes high shear flow disturbances and delay in neointimal coverage as a function of strut to wall detachment distance: implications for the management of incomplete stent apposition.** *Circ Cardiovasc Interv* 2014;7:180–89 CrossRef Medline
10. King RM, Chueh JY, van der Bom IM, et al. **The effect of intracranial stent implantation on the curvature of the cerebrovasculature.** *AJNR Am J Neuroradiol* 2012;33:1657–62 CrossRef Medline
11. Heller RS, Malek AM. **Successful detection of embologenic ulceration in a symptomatic non-hemodynamic intracranial stenosis using C-arm cone beam CT.** *J Neurointerv Surg* 2013;5:e3 CrossRef Medline
12. Struffert T, Lang S, Adamek E, et al. **Angiographic C-arm CT visualization of the Woven EndoBridge cerebral aneurysm embolization device (WEB): first experience in an animal aneurysm model.** *Clin Neuroradiol* 2014;24:43–49 CrossRef Medline
13. Prell D, Kalender WA, Kyriakou Y. **Development, implementation and evaluation of a dedicated metal artefact reduction method for interventional flat-detector CT.** *Br J Radiol* 2010;83:1052–62 CrossRef Medline
14. van der Bom IM, Hou SY, Puri AS, et al. **Reduction of coil mass artifacts in high-resolution flat detector conebeam CT of cerebral stent-assisted coiling.** *AJNR Am J Neuroradiol* 2013;34:2163–70 CrossRef Medline
15. Murayama Y, Viñuela F, Suzuki Y, et al. **Ion implantation and protein coating of detachable coils for endovascular treatment of cerebral aneurysms: concepts and preliminary results in swine models.** *Neurosurgery* 1997;40:1233–43; discussion 1243–44 CrossRef Medline
16. Stidd DA, Theessen H, Deng Y, et al. **Evaluation of a metal artifacts reduction algorithm applied to postinterventional flat panel detector CT imaging.** *AJNR Am J Neuroradiol* 2014;35:2164–69 CrossRef Medline